T-box transcription factor 3 governs a transcriptional program for the function of the mouse atrioventricular conduction system

Rajiv A. Mohan[a,b,1], Fernanda M. Bosada[a,1], Jan H. van Weerd[a], Karel van Duijvenboden[a], Jianan Wang[b], Mathilda T. M. Mommersteeg[c], Ingeborg B. Hooijkaas[a], Vincent Wakker[a], Corrie de Gier-de Vries[a], Ruben Coronel[b], Gerard J. J. Boink[a,b], Jeroen Bakkers[d], Phil Barnett[a], Bas J. Boukens[a,b], and Vincent M. Christoffels[a,2]

[a]Department of Medical Biology, Amsterdam University Medical Centers, University of Amsterdam, 1105 AZ Amsterdam, The Netherlands; [b]Department of Clinical and Experimental Cardiology, Amsterdam University Medical Centers, University of Amsterdam, 1105 AZ Amsterdam, The Netherlands; [c]Burdon Sanderson Cardiac Science Centre, Department of Physiology, Anatomy & Genetics, University of Oxford, Oxford OX1 3PT, United Kingdom; and [d]Hubrecht Institute and University Medical Center Utrecht, 3584 CT Utrecht, the Netherlands

Edited by Christine E. Seidman, HHMI and Brigham and Women's Hospital, and Harvard Medical School, Boston, MA, and approved June 23, 2020 (received for review November 6, 2019)

Genome-wide association studies have identified noncoding variants near *TBX3* that are associated with PR interval and QRS duration, suggesting that subtle changes in *TBX3* expression affect atrioventricular conduction system function. To explore whether and to what extent the atrioventricular conduction system is affected by Tbx3 dose reduction, we first characterized electrophysiological properties and morphology of heterozygous *Tbx3* mutant (*Tbx3*$^{+/-}$) mouse hearts. We found PR interval shortening and prolonged QRS duration, as well as atrioventricular bundle hypoplasia after birth in heterozygous mice. The atrioventricular node size was unaffected. Transcriptomic analysis of atrioventricular nodes isolated by laser capture microdissection revealed hundreds of deregulated genes in *Tbx3*$^{+/-}$ mutants. Notably, *Tbx3*$^{+/-}$ atrioventricular nodes showed increased expression of working myocardial gene programs (mitochondrial and metabolic processes, muscle contractility) and reduced expression of pacemaker gene programs (neuronal, Wnt signaling, calcium/ion channel activity). By integrating chromatin accessibility profiles (ATAC sequencing) of atrioventricular tissue and other epigenetic data, we identified Tbx3-dependent atrioventricular regulatory DNA elements (REs) on a genome-wide scale. We used transgenic reporter assays to determine the functionality of candidate REs near *Ryr2*, an up-regulated chamber-enriched gene, and in *Cacna1g*, a down-regulated conduction system-specific gene. Using genome editing to delete candidate REs, we showed that a strong intronic bipartite RE selectively governs *Cacna1g* expression in the conduction system in vivo. Our data provide insights into the multifactorial Tbx3-dependent transcriptional network that regulates the structure and function of the cardiac conduction system, which may underlie the differences in PR duration and QRS interval between individuals carrying variants in the *TBX3* locus.

Tbx3 | Cacna1g | Ryr2 | atrioventricular conduction system | electrical patterning

The atrioventricular (AV) conduction system facilitates electrical impulse conduction from the atria to the ventricles and coordinates synchronized ventricular activation. T-box transcription factor 3-encoding gene *Tbx3* is specifically expressed in the AV conduction system, and loss-of-function and gain-of-function experiments have demonstrated that *Tbx3* is required for cardiac conduction system development and homeostasis (1). Common variation in the gene desert upstream of *TBX3* has been associated with PR interval and QRS duration (2–6) (*SI Appendix*, Fig. S1). Since the activity of regulatory DNA elements (REs) is largely confined to a topologically associating domain (TAD) (7–12) we hypothesize that the PR and QRS interval-associated variants in the TAD cause subtle differences in *TBX3* expression resulting in altered AV conduction system function. The mechanistic relation between modest *TBX3* expression differences and AV conduction system function has not been investigated yet.

Insight into the transcriptional regulatory network controlling the development and function of the AV conduction system has been largely derived from animal knockout studies on individual transcription factors. These studies uncovered crucial roles for transcription factors including Tbx5, Tbx3, Nkx2-5, and Etv1 (1, 13, 14). Nevertheless, full molecular characterization of the AV conduction system has been hampered by the small size and heterogeneous composition of the AV node and bundle (15, 16). In addition, relevant cell lines modeling this tissue and human AV conduction system samples are insufficiently available. To investigate the repercussions of lower *Tbx3* expression on the AV conduction system, we characterized the AV conduction system morphology and function of *Tbx3* haploinsufficient (*Tbx3*$^{+/-}$)

Significance

Genome-wide association studies have identified common noncoding variants associated with ECG parameters in the *TBX3* locus, suggesting that a modest change in *TBX3/Tbx3* expression level affects heart function. We characterized the morphology, physiology, and gene expression profile of the atrioventricular conduction system in a *Tbx3* haploinsufficient mouse model. We identified Tbx3-dependent regulatory DNA elements active in the atrioventricular conduction system and validated the functionality of these elements in vivo. Using genome editing, we deleted a regulatory DNA element from the mouse genome and show it drives expression of *Cacna1g* in the cardiac conduction system. Our study unveils a Tbx3-dependent gene regulatory network in the AV conduction system that contributes to heart electrophysiology.

Author contributions: R.A.M., F.M.B., R.C., G.J.J.B., J.B., P.B., B.J.B., and V.M.C. designed research; R.A.M., F.M.B., J.H.v.W., J.W., M.T.M.M., I.B.H., V.W., and C.d.G.-d.V. performed research; R.A.M., F.M.B., J.H.v.W., K.v.D, J.W., M.T.M.M., R.C., G.J.J.B., J.B., P.B., B.J.B and V.M.C. analyzed data; and R.A.M., F.M.B., and V.M.C. wrote the paper.

The authors declare no competing interest.

This article is a PNAS Direct Submission.

Data deposition: The data have been deposited with the Gene Expression Omnibus, https://www.ncbi.nlm.nih.gov/geo/ (accession code GSE121465).

[1]R.A.M. and F.M.B. contributed equally to this work.

[2]To whom correspondence may be addressed. Email: v.m.christoffels@amsterdamumc.nl.

This article contains supporting information online at https://www.pnas.org/lookup/suppl/doi:10.1073/pnas.1919379117/-/DCSupplemental.

First published July 16, 2020.

mice, isolated AV nodes and defined their transcriptome, generated a genome-wide chromatin accessibility map of AV conduction system cells, and identified putative Tbx3-dependent AV conduction system REs. To gain insight into the in vivo function of such REs, we deleted an example bipartite RE with a strong epigenetic signature in *Cacna1g* (conduction system-enriched voltage-dependent T-type calcium channel Cav3.1; ref. 17) using genome editing.

Results

Heterozygous Loss of *Tbx3* Causes Postnatal AV Bundle-Bundle Branch Hypoplasia and Affects AV Conduction. We studied the morphology and volume of the AV conduction system of neonatal $Tbx3^{+/-}$ and WT littermates by in situ hybridization on serial sections of hearts. The AV node was defined by the presence of *Hcn4* (Hyperpolarization activated cyclic nucleotide gated potassium channel 4) and absence of *Gja5* (Gap junction protein, alpha 5) expression in the AV junction. The AV bundle and bundle branches (BBs) were identified by coexpression of *Hcn4* and *Gja5* in the AV junction and ventricular septum (16, 18–20). Reconstructing and measuring the volumes of the $Hcn4^{+}Gja5^{-}$ AV node and $Hcn4^{+}Gja5^{+}$ AV bundle-BBs using three-dimensional (3D) quantitative morphometric analysis showed that AV node, AV bundle, and BBs were not different between neonatal WT and $Tbx3^{+/-}$ hearts (Fig. 1 *A* and *B*). In contrast, AV bundle-BBs of 2-mo-old $Tbx3^{+/-}$ mice were hypoplastic, while the AV node remained similar in size to WT littermates (Fig. 1 *C* and *D*), thus indicating that AV bundle-BBs hypoplasia in $Tbx3^{+/-}$ mice develops after birth. We found no evidence of apoptosis (cleaved caspase-3) in hypoplastic AV bundles of $Tbx3^{+/-}$ mice at postnatal day (P) 28 (*SI Appendix*, Fig. S2).

Next, we recorded electrocardiograms (ECGs) in vivo from 2-mo-old mice and ex vivo from hearts and found significantly shorter PR interval (WT 27.57 ± 0.62 ms and *Tbx3* ± 24.33 ± 0.22 ms) and prolonged QRS duration (WT 8.15 ± 0.62 ms and *Tbx3* ± 10.33 ± 0.44 ms) in *Tbx3* ± mutant hearts ex vivo. In contrast, there were no differences in vivo (PR: WT 33.34 ± 1.27 ms and *Tbx3* ± 32.27 ± 1.05 ms; QRS: 10.35 ± 0.41 ms and *Tbx3* ± 10.70 ± 0.51 ms) (Fig. 1*E*). Furthermore, we did not observe delta waves in ECG traces (Fig. 1*F*). To test whether the autonomic nervous system concealed a possible phenotype in vivo, we recorded ECGs in the presence of propranolol and atropine. QRS duration in WTs did not change after autonomic blockade (before, 9.07 ± 0.30 ms; after, 8.95 ± 0.40 ms), whereas $Tbx3^{+/-}$ mutants had showed a trend toward QRS prolongation from 9.07 ± 0.25 ms to 9.59 ± 0.38 ms ($P = 0.08$) (*SI Appendix*, Fig. S3). Optical mapping of isolated Langendorff-perfused hearts showed delayed apical activation at the dorsal side in $Tbx3^{+/-}$ mutants compared to controls (Fig. 1*G*). The anterior side showed two near simultaneous epicardial breakthroughs in WT hearts. In mutant hearts, multiple small breakthroughs separated by areas of late activation were present (Fig. 1*G*). The epicardial activation patterns indicate a slower and less homogeneous activation of the ventricular chambers possibly as a consequence of the AV bundle/BB hypoplasia. Together, these findings reveal previously underappreciated changes in AV conduction system morphology and function in a *Tbx3* haploinsufficient mouse model.

Gene Expression Profiles of WT and $Tbx3^{+/-}$ AV Nodes. Deregulation of the AV nodal gene program is likely to contribute to PR interval shortening. Therefore, we characterized the transcriptomes of $Tbx3^{+/-}$ and WT AV nodes. We performed fluorescence-guided laser capture microdissection to isolate labeled AV node tissue from P8–10 unfixed cryosections (Fig. 2*A*). To specifically identify AV nodes of WT and *Tbx3* heterozygotes, we generated $Tbx3^{+/+}$;*BAC-Tbx3-Egfp* and $Tbx3^{+/CreERT2}$;*BAC-Tbx3-Egfp* mice (21). *BAC-Tbx3-Egfp* mice express Egfp in the compact AV node, but not in the other tissues surrounding the AV node (22).

As a first validation, we examined the expression of established AV nodal, chamber, and ventricular conduction system marker genes (15, 16, 18, 22–24). *Hcn4*, *Cacna1g* (Calcium channel, voltage-dependent, T-type, alpha 1G subunit), *Cacna2d2* (Calcium voltage-gated channel auxiliary subunit α2-δ2), and *Igfbp5* (Insulin like growth factor binding protein 5) were highly enriched in our AV nodal samples. In contrast, genes specific for atrial and ventricular chamber myocardium, and ventricular conduction system, *Nppa* (Natriuretic peptide type A), *Gja1* (Gap junction protein, alpha 1), and *Gja5*, were virtually absent in our samples (Fig. 2*C*) (16, 24, 25).

Transcriptomic analysis revealed that 892 transcripts were differentially expressed in $Tbx3^{+/-}$ AV nodes (12,033 total transcripts detected, $P < 0.05$). Of these, 409 genes were down-regulated, (e.g., *Hcn1, Hcn4, Cacna2d2, Kcnh2*, and *Cacna1g*) and 483 genes were up-regulated (e.g., *Myh6, Scn5a, Kcne1*, and *Ryr2*; Fig. 2*B* and see *SI Appendix*, Table S1). Unsupervised hierarchical clustering of the differentially expressed genes resulted in two primary groups based on genotype (Fig. 2*D*). Gene ontology (GO) term and Kyoto Encyclopedia of Genes and Genomes (KEGG) pathway analysis identified genes involved in Wnt signaling, neuronal, and voltage-gated ion channel activity to be overrepresented in the down-regulated gene set of $Tbx3^{+/-}$ AV nodes. Neuronal gene profiles are found in the AV conduction system (22), and Wnt signaling plays crucial roles in its development (26–28). Genes important for mitochondria, metabolism, and cardiac muscle contraction were found to be overrepresented in the up-regulated genes (Fig. 2*D*). As chamber (working) cardiomyocytes have more mitochondria and better developed sarcomeric structures and sarcoplasmic reticula compared to nodal cells (29–31), it stands to reason that genes associated with working myocardial gene programs are up-regulated in AV nodal cells of $Tbx3^{+/-}$ mice. However, the overall changes in expression are small and are therefore unlikely to affect detectable AV nodal properties. Indeed, we found no difference in mitochondrial abundance (CoxIV immunolabeling) between WT and $Tbx3^{+/-}$ AV nodes (Fig. 2*E* and see *SI Appendix*, Fig. S4). Interestingly, genes involved in calcium homeostasis were found in both the down-regulated and up-regulated gene sets. This could reflect the existence of complex Tbx3-dependent transcriptional modulation that controls AV node function.

To gain further insight into the transcriptional regulatory hierarchy in the AV node, we cross-referenced our dataset with a catalog of genes encoding transcription factors (32). In total, transcripts of 710 transcription factor-encoding genes were expressed in the AV node samples. The top 50 highest expressed transcription factor genes include *Tbx5*, *Tbx3*, *Tbx20*, *Mef2a*, *Gata4*, *Gata6*, and *Prox1*. Interestingly, *Tbx5* and *Prox1* were down-regulated in $Tbx3^{+/-}$ AV nodes (Fig. 2*B*) (33, 34). Together, our data indicate $Tbx3^{+/-}$ AV nodes acquired a modest working myocardial gene program while maintaining pacemaker properties.

Identification of Tbx3-Dependent AV Conduction System Regulatory Elements. To identify regulatory elements active in the AV conduction system cardiomyocytes, we used Assay for Transposase-Accessible Chromatin (ATAC)-sequencing (seq) (35) on fluorescence-activated cell sorting (FACS)-purified $Venus^{+}$ cells from microdissected AV junctions of $Tbx3^{+/Venus}$ fetuses (Fig. 3*A*). Peak calling (*SI Appendix*, Fig. S5*A*) identified 54,273 accessible regions, of which 41% overlapped with an available histone H3K27ac ventricular cardiomyocyte chromatin immunoprecipitation (ChIP)-sequencing dataset (36) (Fig. 3*B* and see *SI Appendix*, Fig. S5*A*). As expected, the overlap between ATAC-seq data from ventricular cardiomyocytes (37) and this

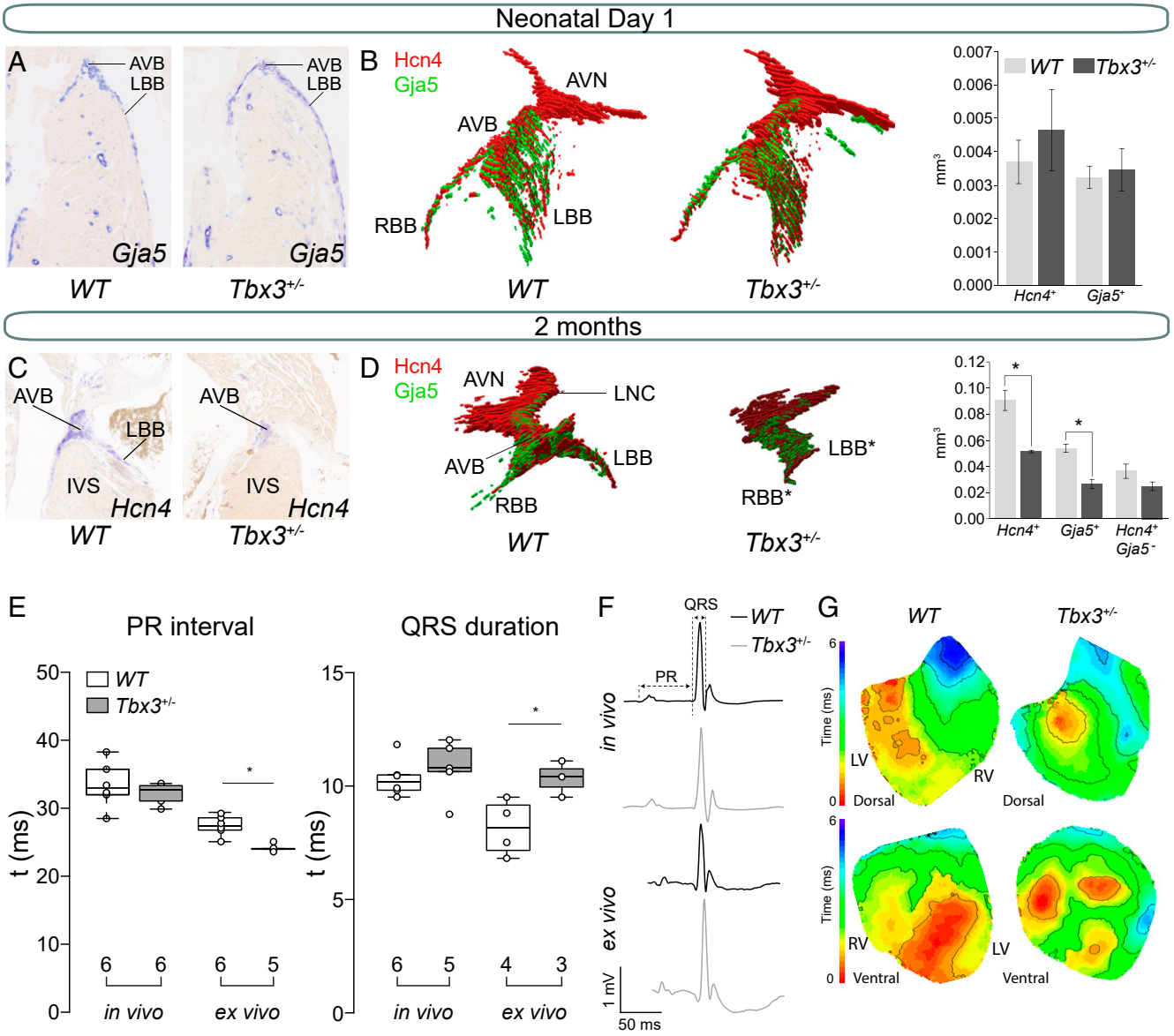

Fig. 1. Hypoplasia of the AV bundle-bundle branches and conduction disturbances in adult *Tbx3*$^{+/-}$ mice. (*A*) Representative sections of newborn WT and *Tbx3*$^{+/-}$ AVB-BBs. (*B*) Examples of a reconstruction of newborn WT and *Tbx3*$^{+/-}$ AV conduction system showing expression of *Hcn4* (red) and *Gja5* (green). Average volumes of *Hcn4* (AV conduction system) and *Gja5* (AV bundle and bundle branches) and *Hcn4*$^{+}$-*Gja5*$^{+}$ (AV node) expression domains in the AV conduction system of three WT (dark gray) and three *Tbx3*$^{+/-}$ (light gray) mice. Error bars represent SEM. *$P < 0.05$ was considered significant using a two-tailed Student's *t* test. (*C*) Representative sections of 2-mo-old WT and *Tbx3*$^{+/-}$ AVB-BBs. (*D*) Example of a reconstruction of WT AV conduction system showing expression of *Hcn4* (red) and *Gja5* (green). Average volumes of *Hcn4*$^{+}$, *Gja5*$^{+}$, and *Hcn4*$^{+}$-*Gja5*$^{-}$ expression domains in the AV conduction system of three WT (dark gray) and three *Tbx3*$^{+/-}$ (light gray) mice. Error bars represent SEM. (*E*) Boxplots visualizing the individually measured and average PR interval and QRS duration in vivo and ex vivo. Numbers below boxplot reflect the number of animals measured. (*E*) Boxplots visualizing the individually measured and average PR interval and QRS duration in vivo and ex vivo. (*F*) In vivo and ex vivo ECG traces from WT and *Tbx3*$^{+/-}$ mice. (*G*) Dorsal and ventral activation maps from WT and *Tbx3*$^{+/-}$ mice based on optical mapping. *$P < 0.05$ was considered significant using two-way ANOVA. AVB, atrioventricular bundle; AVN, atrioventricular node; IVS, interventricular septum; LBB, left bundle branch; LNC, lower nodal cells; RBB, right bundle branch.

H3K27ac ChIP-seq dataset was much broader (70%) (Fig. 3*B*), suggesting that the AV conduction ATAC-seq dataset could be useful to pinpoint AV conduction system-specific REs. Indeed, three previously established AV conduction system-specific REs (12, 38, 39) were readily identified in this dataset (*SI Appendix*, Fig. S5 *B* and *C*).

Next, we intersected our AV conduction system ATAC-seq with available cardiac Tbx3 and Tbx5 ChIP-seq datasets (Tbx3 and Tbx5 share DNA binding sites), as well as the recently improved EMERGE cardiac enhancer prediction tool (40–43) to identify candidate Tbx3-dependent, AV conduction system specific REs. We chose to focus on two loci harboring genes representative of up-regulated and down-regulated transcripts in *Tbx3*$^{+/-}$ AV nodes: *Ryr2* (up), and *Cacna1g* (down). Both genes are found in loci containing variants associated with PR-interval (44) and had straightforward epigenomic signatures.

Ryr2 encodes the Ryanodine receptor 2, which plays a role in calcium homeostasis (45) and is enriched in chamber myocardium (15). In this locus, we selected 19 regions as candidate REs based solely on chromatin accessibility in the AV conduction

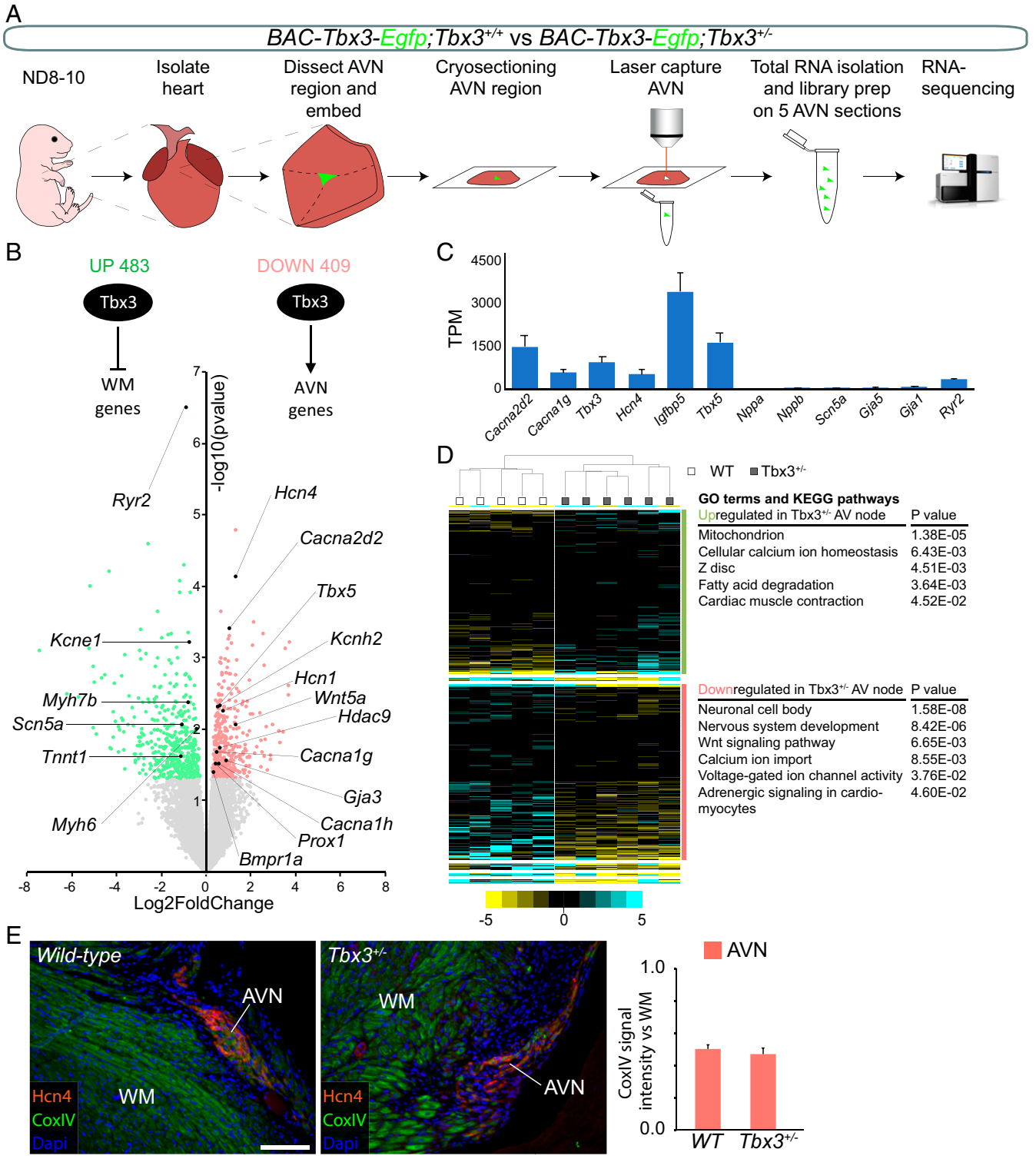

Fig. 2. Tbx3 maintains pacemaker and conduction properties in the AV node. (*A*) Approach to obtain and define transcriptomes of WT and *Tbx3*$^{+/-}$ AV nodes. (*B*) Volcano plot of normalized expression levels in WT AV nodes over *Tbx3*$^{+/-}$ AV nodes. All significantly up-regulated genes are labeled green, and all significantly down-regulated genes are labeled red. $P < 0.05$ (red and green), $P < 0.1$ (light red and light green). (*C*) Average WT expression levels (in TPM) of conduction system and chamber genes. (*D*) Unsupervised hierarchical clustering of genes differentially expressed between *Tbx3*$^{+/-}$ AV nodes and WT AV nodes. GO terms and KEGG pathways associated with up-regulated (green) and down-regulated (red) genes in *Tbx3*$^{+/-}$ AV nodes. (*E*) Representative immunostaining for Hcn4 (red), CoxIV (green), and nuclei (blue). Graph shows quantification of CoxIV signal intensity in AVN normalized to WM in WT and *Tbx3*$^{+/-}$ sections ($n = 3$). AVN, AV node; WM, working myocardium. (Scale bar: 10 μm.)

system cardiomyocytes and scored these regions for Tbx3 and Tbx5 occupancy derived from cardiomyocyte-specific datasets, and whether they were predicted to be a cardiac enhancer by EMERGE (41–43) (*SI Appendix*, Fig. S6). Four of these regions (Fig. 3*C*) were selected for transfection luciferase assays in HL-1, an atrial cardiomyocyte-like cell line, and Cos-7, a noncardiomyocyte

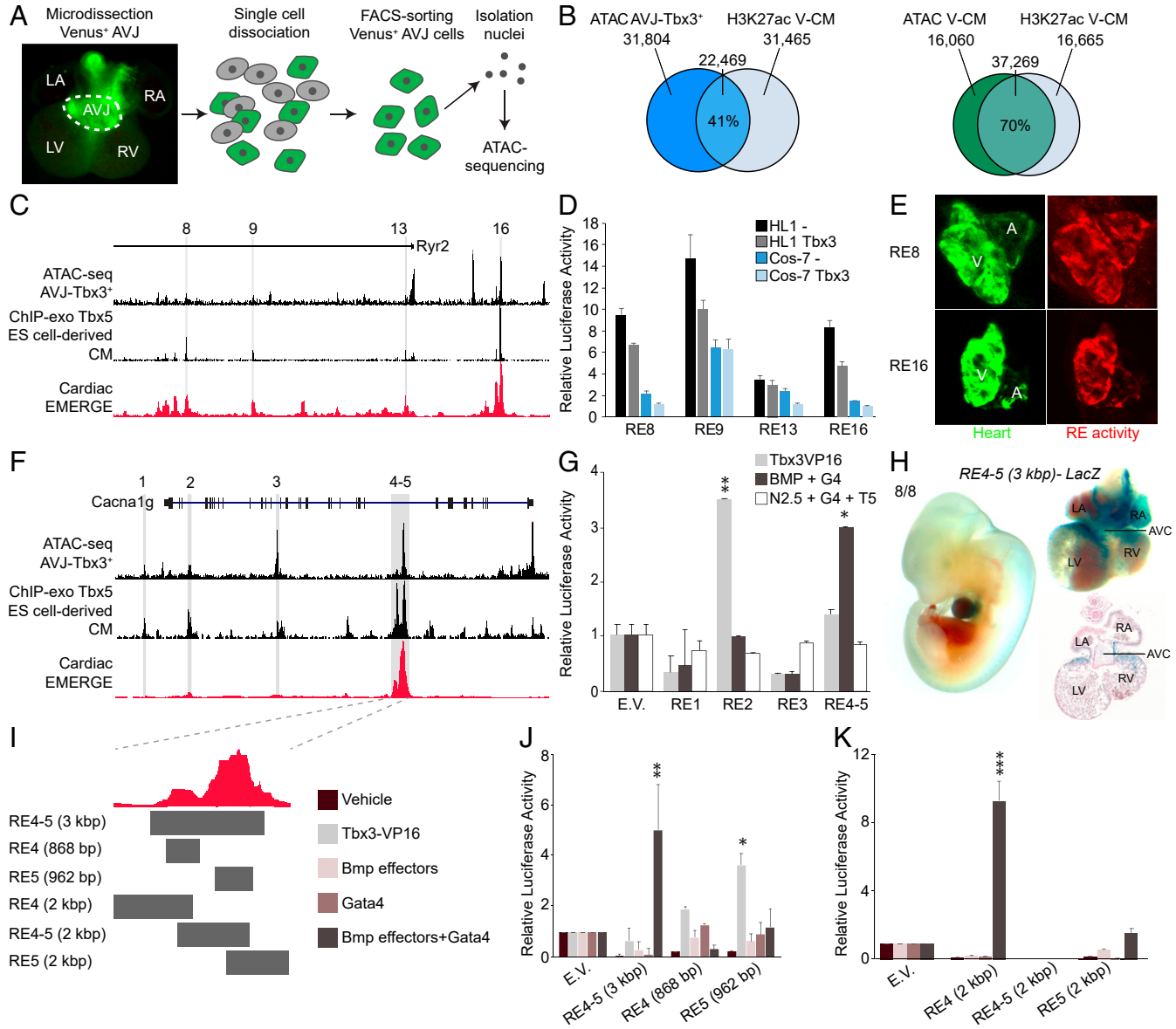

Fig. 3. Identification and functional testing of Tbx3-dependent REs. (*A*) Strategy to assay the accessible chromatin profiles in E12.5–E14.5 AV conduction system cardiomyocytes using ATAC-seq. (*B*) Venn diagrams showing overlap between Venus$^+$ AV conduction system ATAC-seq signals (*Left*) or ventricular cardiomyocyte (V-CM) ATAC-seq signals (*Right*) and ventricular cardiomyocyte H3K27ac enrichment. (*C*) Genomic region around transcription start site of *Ryr2* showing relevant ATAC-seq and ChIP-seq signals and four potential REs. (*D*) Basal activity (–) and Tbx3 repressed activity of the four regions in transiently transfected HL1 (black and gray) and Cos-7 (dark and light blue) cells. Relative luciferase activity was normalized to the empty vector. (*E*) In vivo RE8 and RE16 activity pattern in 5 d postfertilization Attp^{2P} zebrafish embryos. A, atrium; CM, cardiomyocytes; V, ventricle. (*F*) A large region including *Canca1g* locus showing relevant ATAC-seq and ChIP-seq signals and five potential REs. (*G*) Basal activity of REs and activity in the presence of several forms of stimuli included by cotransfection. (*H*) E11.5 RE4-5-*LacZ* transient transgenic embryo showing expression in the heart and specifically in the AV canal. Eight of eight transient transgenic embryos had expression in the heart. (*I*) Tested smaller fragments of RE4-5. (*J* and *K*) Basal activity of REs and activity in the presence of several forms of stimuli included by cotransfection. For all luciferase assays, relative luciferase activity was normalized to the empty vector. *$P < 0.05$ was considered significant using a two-tailed Student's *t* test. **$P < 0.01$, ***$P < 0.001$. AVB, AV bundle; AVC, AV canal; IVS, interventricular septum; LA, left atrium; LBB, left bundle branch; LV, left ventricle; RA, right atrium; R-AVRB, right AV ring bundle; RBB, right bundle branch; RV, right ventricle.

cell line. HL-1 cells express *Tbx5* and *Ryr2*, but not *Tbx3*, and based on transcriptome analysis, are similar to fetal right atrial cardiomyocytes (*SI Appendix*, Fig. S7). All regions were more active in HL-1 than in Cos-7 cells (Fig. 3*D*), thus implying the candidate REs are cell-type specific. Additionally, the activity of three of the REs was repressed by TBX3 (Fig. 3*D*). We determined the spatial activity of RE8 and RE16 in a zebrafish reporter assay and confirmed that both regions show specific activity in the atrium and ventricles of the fish heart and not in other tissues (Fig. 3*E*). Our data indicate that these *Ryr2* REs are active in chamber myocardium and are repressed by Tbx3.

The second Tbx3 target we chose to study is *Cacna1g*. This gene encodes the T-type calcium channel Cav3.1, is important for calcium homeostasis, is specifically expressed throughout development and adulthood in the conduction system in an expression pattern similar to *Tbx3* (*SI Appendix*, Fig. S8) (46), and was down-regulated in *Tbx3*$^{+/-}$ AV nodes (Fig. 2*B*).

Furthermore, previous studies have demonstrated that *Cacna1g* is induced by Tbx3 (47) and knockout mice present with PR interval phenotypes (17). We selected eight chromatin regions accessible in the $Tbx3^+$ AV junction and then scored each region for Tbx3 and Tbx5 occupancy and EMERGE cardiac enhancer prediction signal (*SI Appendix*, Fig. S9). A previous study showed that many AV canal-specific REs are GATA-dependent switches; synergistic activity of Gata4 and Bmp2/Smad signaling results in H3K27 acetylation and transcription of AV-specific target genes (48). Therefore, we tested the responsiveness of five of the candidate regions to Tbx3, Gata4, and/or Bmp signaling effectors using transfection luciferase assays in HEK 293 cells (Fig. 3*F*). We found that RE2 was responsive to Tbx3 and RE4-5 to Bmp signaling effectors (constitutively active Alk3, Smad1,

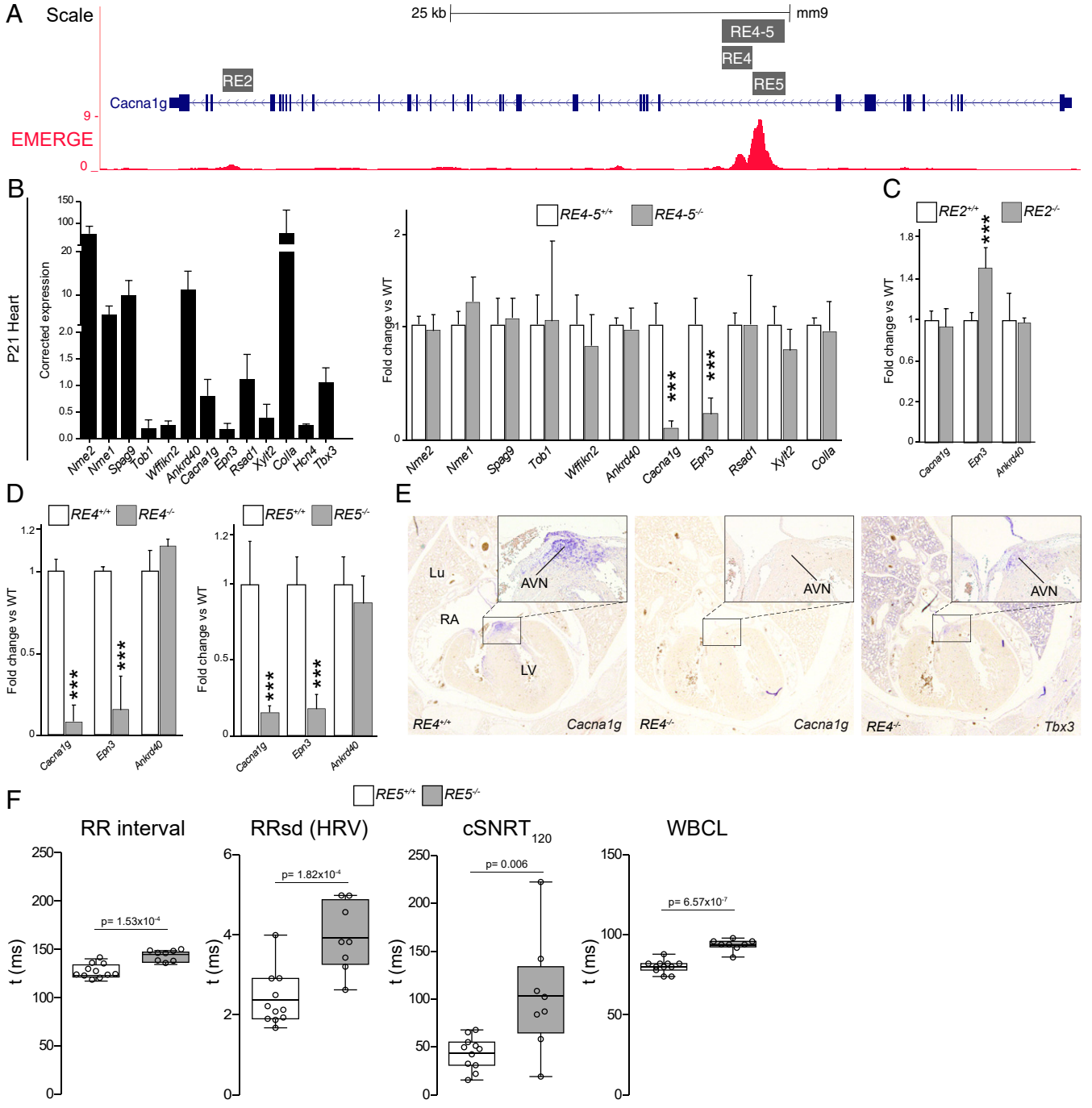

Fig. 4. Deletion of RE4-5, RE4, or RE5 abolishes expression of *Cacna1g* in the heart. (*A*) CRISPR/Cas9 deletions in the context of EMERGE signal. (*B*) Relative expression of TAD genes from P21 WT hearts ($n = 7$) determined by qPCR with *Tbx3* and *Hcn4* shown as cardiac conduction system markers (*Left*). Fold change expression levels of TAD genes in P21 $RE4\text{-}5^{-/-}$ ($n = 8$) vs. WT littermates (*Right*). (*C* and *D*) Relative expression of *Cacna1g*, *Epn3*, and *Ankrd40* as a control in $RE2^{-/-}$ ($n = 6$) (*C*) and $RE4^{-/-}$ ($n = 7$) and $RE5^{-/-}$ ($n = 8$) (*D*). (*E*) Histological sections of WT and $RE4^{-/-}$ E17.5 mice stained for *Cacna1g* and *Tbx3*. (*F*) Boxplots visualizing the individually measured and average RR interval, RRsd, cSNRT, and WBCL. $^*P < 0.05$ was considered significant one-way ANOVA (*B–D*) or Student's *t* test (*F*) ($^{**}P < 0.01$; $^{***}P < 0.001$); AVN, AV node; cSNRT, corrected sinus node recovery time; HRV, heart rate variation; Lu, lung; LV, left ventricle; RA, right atrium; RRsd, RR interval SD; WBCL, Wenckebach cycle length.

Smad4, and Gata4) (Fig. 3*G*), whereas none of the REs were responsive to other cardiogenic transcription factors (Nkx2.5, Gata4, and Tbx5). This result suggests that RE2 and RE4-5 are specifically active in the AV conduction system (48). Next, we examined the spatial activity of RE4-5 in transient transgenic embryos and found it was active in the E11.5 AV canal (precursor of the AV conduction system) in 8/8 transgenic embryos, with 3/8 showing no activity outside the heart (Fig. 3*H*). However, the individual RE4 or RE5 fragments failed to drive reporter expression in the hearts of five transgenic embryos per fragment (*SI Appendix*, Fig. S10), indicating the function of RE4 and RE5 is interdependent. To further characterize this behavior, we tested the responsiveness of RE4-5 subfragments in luciferase assays (Fig. 3 *I–K*). RE5 was responsive to Tbx3-VP16 (Fig. 3*J*). In contrast, a fragment spanning most of RE4 was synergistically induced by Bmp signaling effectors and Gata4, but not by either of these factors alone. A 1.5-kbp fragment including the junction of RE4 and RE5 and most of RE5 could not be stimulated by any of the transfected effectors (Fig. 3*K*). These results confirm that RE4-5 together drive AV canal expression in vivo, and suggest the individual parts integrate different AV canal-associated transcriptional mechanisms.

Functional Analysis of a Bipartite AV Conduction System Regulatory Element In Vivo. To determine if the Tbx3-dependent REs identified in the *Cacan1g* locus are required for expression in the AV conduction system, we deleted RE2 and RE4-5 from the mouse genome using CRISPR/Cas9 (Fig. 4*A* and see *SI Appendix*, Fig. S11*A*). Homozygous mice for all deletions developed and bred normally and were morphologically indistinguishable from their WT littermates. Because REs are known to regulate expression of distally located genes within a TAD (7–9), we analyzed cardiac transcript levels of genes within the same TAD as *Cacna1g* by qPCR (*SI Appendix*, Fig. S11*A*). Heart samples from P21 mice homozygous for a 3-kbp deletion spanning RE4-5 ($RE4\text{-}5^{-/-}$) showed a 90 and 75% down-regulation of *Cacna1g* and *Epn3* transcripts, respectively, when compared to WT littermates, while all other genes within the TAD were unaffected (Fig. 4*B*). In contrast, isolated brain samples showed no significant changes in transcript levels (*SI Appendix*, Fig. S11*B*), indicating that RE4-5 is tissue-specific. Deletion of RE2 resulted in modest up-regulation of *Epn3* expression only, thus suggesting that this RE is dispensable for cardiac-specific *Cacna1g* expression (Fig. 4*C*).

To test whether the function of RE4 and RE5 is interdependent, as suggested by the in vivo RE assays, we generated mouse lines in which RE4 and RE5 were deleted individually (Fig. 4*A* and see *SI Appendix*, Fig. S11*A*). Homozygous removal of either genomic region resulted in down-regulation of *Cacna1g* specifically in the heart to levels comparable to those observed in hearts of $RE4\text{-}5^{-/-}$ mice (Fig. 4*D*). To confirm this finding, we analyzed the expression pattern of *Cacna1g* by in situ hybridization. Sections of E17.5 $RE4^{-/-}$ or $RE5^{-/-}$ mice showed no staining for *Cacna1g* transcripts in the heart, whereas expression of *Tbx3* was unchanged (Fig. 4*E*; not shown for $RE5^{-/-}$). $RE5^{-/-}$ mice showed bradycardia (Fig. 4*F*), similar to *Cacna1g* homozygous mutants (17), further demonstrating functional loss of *Cacna1g* in the conduction system of $RE5^{-/-}$ mutants. Additionally, $RE5^{-/-}$ mice showed higher heart rate variation (HRV) when compared to WT littermates (Fig. 4*F*). We observed slower corrected sinus node recovery times (cSNRTs) and higher Wenckebach cycle length in $RE5^{-/-}$ mice, consistent with sinus and AV node dysfunction (Fig. 4*F*). Together, our data show that RE4-5 functions as a bipartite, AV conduction system-specific RE that is essential to drive expression of *Cacna1g*.

Discussion

We demonstrate that heterozygous loss of *Tbx3* shortens AV nodal conduction (PR interval) and prolongs QRS duration. The haploinsufficiency causes modest changes in expression of genes associated with AV nodal identity and function. Additionally, *Tbx3* heterozygous mice fail to maintain AV bundle-BBs structure after birth. We show that REs in the *Ryr2* locus are active in the chambers and are repressed by Tbx3. Further, we found a bipartite RE in the *Cacna1g* locus that is active in the $Tbx3^{+}$ AV conduction system where it selectively controls expression of *Cacna1g* and *Epn3* in vivo and none of the >15 other genes in the TAD.

Genome-wide association studies have identified common noncoding variants associated with PR interval and QRS duration in a 1-Mbp TAD that only harbors *TBX3* (2–6, 10, 12) (*SI Appendix*, Fig. S1); we infer that these variants affect the function of REs controlling *TBX3* expression. Currently, this assumption is difficult to validate; expression quantitative trait loci analysis is not yet feasible due to the low number of human AV conduction system samples available, extremely low expression in other cardiac cells, and the unavailability of reliable human AV conduction system cell models.

Tbx3 mutants showed prolonged QRS, which may result from the hypoplastic AV bundle and BBs (49). Apoptosis does not seem to underlie the AV bundle-BBs hypoplasia, and less proliferation after birth is unlikely to be the culprit, because the AV bundle shows very limited proliferation from early fetal stages onwards (49–51), and cardiomyocyte proliferation rates, in general, decline to negligible levels shortly after birth (52–54).

Using a series of *Tbx3* hypomorphic and deficient alleles, Frank et al. found that Tbx3 is required for the function of the conduction system in a dosage-sensitive manner (55). Mice expressing 30% or less of WT transcript levels developed severe arrhythmias, and surviving adults displayed PR shortening. $Tbx3^{+/-}$ mutants in our study show PR interval shortening in addition to AV bundle-BBs hypoplasia and prolonged QRS duration. We speculate that the PR interval shortening in *Tbx3* haploinsufficient mice results from AV bundle hypoplasia in addition to the modest deregulation of many genes implicated in the electrophysiological properties of AV nodal cells (e.g., calcium channels/handling proteins, Hcn channels, gap junction subunits, sodium channels, potassium channels). Additional insight into the quantitative changes and functional interactions between the dysregulated targets is required to understand the observed net effect.

Tbx3 and its paralog and functional homolog *Tbx2* have been implicated in accessory AV pathway formation (28, 55–57), which could result in conduction abnormalities consistent with the phenotypes found in $Tbx3^{+/-}$ mutants. However, we found no delta waves in ECG traces, and optical mapping showed no early breakthrough at the base of the left ventricles in controls and mutants (Fig. 1). Therefore, it is unlikely that the presence of an accessory pathway underlies the observed electrophysiological phenotypes in $Tbx3^{+/-}$ mutants. Instead, AV bundle-BBs hypoplasia is more likely to explain the conduction changes and is in line with the observed in $Tbx3^{+/-}$ mutants. The shorter PR interval in $Tbx3^{+/-}$ mutants was only present ex vivo, and neither in vivo nor with chemical ANS blockade. The autonomic nervous system has a large impact on AV conduction (58). We consider it possible that in $Tbx3^{+/-}$ mutants, the autonomic nervous system activity partially compensated for the modest defects caused by heterozygous loss of *Tbx3*, explaining the absence of PR interval changes in vivo. Therefore, we suggest that intrinsic AV nodal conduction is affected in *Tbx3* mutants.

Many transcription factors in addition to Tbx3 have been implicated in the development and function of the AV conduction system, including Nkx2-5, Tbx5, Prox1, Hopx, Irx3, and

Gata4/6 (reviewed in refs. 1, 13, and 14). Several of these factors target the same genes and interact with each other, both physically and genetically, thus substantiating that they form a transcriptional network in the AV conduction system. Tbx3 and Tbx5 are coexpressed in the entire AV conduction system, and both function in highly dose-sensitive manners (33, 49, 55, 58–62). Tbx3 likely competes with Tbx5 for DNA binding sites (41). Tbx5 stimulates a fast-conduction gene program (e.g., *Scn5a* and *Gja5*) in the AV bundle (61), whereas Tbx3 suppresses it, while stimulating the nodal (pacemaker-specific) program (e.g., *Hcn4* and *Cacna1g*) (47, 63, 64), suggesting a finely tuned balance between these factors (51).

Unexpectedly, *Tbx5* was down-regulated in *Tbx3* haploinsufficient AV nodes. Whether Tbx5 directly regulates the expression of *Tbx3* in the AV node, as it does in the sinus node, is unknown (60). Our data show that the expression of other transcription factors in the AV node is largely unaffected by *Tbx3* haploinsufficiency. This suggests that while *Tbx3* reduction causes deregulation of genes directly involved in cellular properties, such as ion channels, it has a minimal impact on the transcription factor networks in this tissue.

We mapped the accessible chromatin in fetal AV canals, which contain the embryonic AV nodal cells, and integrated these data with Tbx5 and Tbx3 occupancy profiles and EMERGE cardiac enhancer prediction signal to identify candidate Tbx3/5-regulated REs on a genome-wide scale. We then selected two example loci, *Ryr2* and *Cacna1g*, for further examination. *Ryr2* expression is chamber-enriched and induced in the AV node of $Tbx3^{+/-}$ mice, whereas *Cacna1g* is conduction system-specific and reduced in $Tbx3^{+/-}$ mutants, and both loci contain PR interval-associated variants (44). Two REs in close proximity to the *Ryr2* promoter were active in the fish cardiac chambers and were active in an atrial-like cell line where their activity was repressed by Tbx3. The repressor function of Tbx3 is well described (65). This suggests that Tbx3 may directly control expression of *Ryr2* and other chamber-enriched genes in the AV conduction system through these classes of REs.

Cacna1g is expressed specifically in the AV conduction system in a pattern resembling that of *Tbx3*, and it is important for AV node cell automaticity (17). Previously, *Cacna1g* expression was found to be induced by Tbx3 (47, 64) and was found to be down-regulated in $Tbx3^{+/-}$ AV nodes in this study. Congruently, we identified an intronic bipartite *Cacna1g* RE accessible in the $Tbx3^{+}$ AV junction, occupied by Tbx5, Tbx3, Nkx2-5, and Gata4, and acetylated H3K27, a mark associated with active REs (*SI Appendix*, Fig. S9). The bipartite RE and both its individual components were required for cardiac expression of *Cacna1g* in vivo, whereas the entire RE but not its components was sufficient to drive AV conduction system expression in the mouse embryo. Furthermore, while REs have been observed to act redundantly in vivo (8, 66), this RE seems to integrate all of the regulatory information required to drive *Cacna1g* in the entire conduction system. The slower heart rates observed in RE5 mutants can be attributed to loss of *Cacna1g* in the sinus node—also demonstrated by slower cSNRTs (Fig. 4*F*) and studies of a *Cacna1g* knockout model (17). Nevertheless, our data are unable to correlate the observed heart rate variation in mutants solely to sinus or AV node dysfunction, and we speculate the phenotype could be a consequence of deficiencies in both compartments of the cardiac conduction system.

Finally, the activity of REs is usually limited to the TAD they share with potential target genes, in which they can act on multiple target promoters (7–9). Our study reveals that in the context of the TAD, which contains >15 genes, the RE selectively and dominantly regulates *Cacna1g* in vivo. The expression of only one distal gene, *Epn3*, was affected by the deletion of the REs. *Epn3* (Epsin 3) is expressed at very low levels in cardiac tissue and its function has not been associated with the heart. In contrast, RE2, also in the *Cacna1g* gene, was dispensable for *Cacna1g* expression, but was involved in regulation of *Epn3*, further illustrating the complexity of the regulatory landscape.

How Tbx3/5-occupied AV conduction REs such as the one we identified in *Cacna1g* are stimulated by Tbx3 remains unclear. Previously, AV canal REs were found to function as switches activated by Gata4 and Bmp signaling effectors and histone H3K27 acetylation activity in the AV canal and repressed by Gata4, Hey1/2, and HDACs in the chambers (48). In vitro, one part of the bipartite RE was stimulated by Gata4 and Bmp signaling effectors, suggesting parts of this RE function similarly. The other part of the composite RE was responsive to Tbx3 and occupied by Tbx3 and Tbx5 based on cardiac ChIP-seq data, suggesting it mediates the response to the Tbx3/5 ratio in the AV conduction system. Together, these data suggest that while each part of the RE responds to a different AV conduction system-relevant regulatory signaling system, these signals need to be combined and integrated for the bipartite enhancer to function in vivo.

We conclude that Tbx3 dose-dependently governs a transcriptional program that provides an AV conduction system-typical identity. Additionally, our study contributes a possible explanation how individuals carrying common noncoding variants in the *TBX3* locus have an increased risk for differences in the duration of PR and QRS intervals (Fig. 5).

Materials and Methods

For detailed methods, see *SI Appendix*.

Cryosectioning and Laser Capture Microdissection. Hearts from *Tbx3*$^{+/+}$*;BAC-Tbx3-Egfp* and *Tbx3*$^{+/CreERT2}$*;BAC-Tbx3-Egfp* ND8-10 pups were removed, the AV node region microdissected (based on fluorescence) and immediately embedded in O.C.T. (Tissue-Tek, 621232) in the −20 °C for 10 min. Cryosectioning was performed with a cryostat (Leica Biosystems, CM1950), and AV node tissue was sectioned at a thickness of 8 μm. Five consecutive sections were collected and mounted onto PEN-membrane coated slides (MembraneSlide 1.0 PEN, Carl Zeiss Microscopy, 415190-9041-001). Microdissection was performed immediately afterward with a Laser Microdissection Microscope (Leica Microsystems, LMD6), and the AV node was identified visually based on fluorescence. Laser power, aperture, and speed of the laser varied from experiment to experiment. Microdissected AV node tissue sections were collected in a tube containing the lysis buffer of the PicoPure RNA isolation kit (Thermo Fisher Scientific, KIT0204) and the first step of the manufacturer's protocol conducted before the samples were stored at −80 °C.

RNA Isolation and Sequencing of Laser Capture Microdissected AV Node Sections. Total RNA was isolated from neonatal day 8–10 AV node sections according to the manufacturer's protocol of the PicoPure RNA isolation kit (Thermo Fisher Scientific, KIT0204) with an on-column DNase treatment (RNase-free DNase, Qiagen, 79254). RNA integrity and concentration were

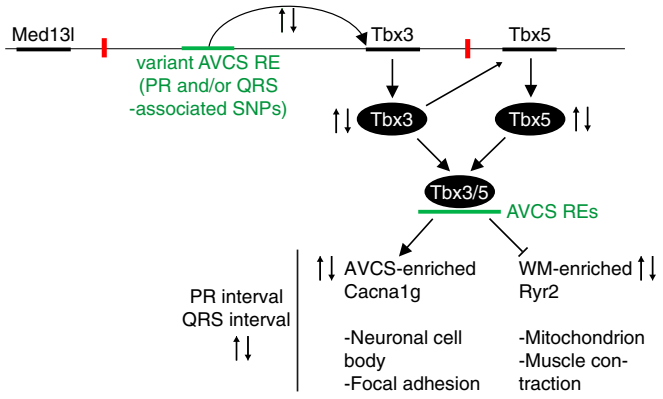

Fig. 5. A model illustrating how variants in REs that affect *Tbx3* expression in the AV conduction system may regulate PR and QRS duration.

determined using the Bioanalyzer RNA 6000 Pico materials (Agilent Technologies, 5067-1513 and 5067-1535). The Ovation RNA-seq system V2 (Nugen, 7102-32) was used for cDNA synthesis with a RNA input between ~300 and 2,000 pg. The quality of the cDNA library was determined with a Bioanalyzer DNA 7500 kit (Agilent Technologies, 5067-1506), the purity with the Nanodrop (Isogen Life Science, ND-1000) and the quantity with the Qubit dsDNA HS kit (Thermo Fisher Scientific, Q32854). RNA-seq libraries were made using Ovation Ultralow Library System V2 (Nugen, 0344-32) and sequenced on the HiSeq 4000 (Illumina). The raw data have been deposited with the Gene Expression Omnibus (https://www.ncbi.nlm.nih.gov/geo/) under accession code GSE121465.

Assay for Transposase-Accessible Chromatin Sequencing. *Tbx3*$^{+/Venus}$ hearts were dissected from embryonic day (E) 12.5–E14.5 embryos and enriched for AV conduction system tissues by microdissection. Tissue samples were dissociated into a single-cell suspension using 0.05% Trypsin/EDTA (Thermo Fisher Scientific, 25300-054) for 15 min at 37 °C. Dissociated cells were resuspended in DMEM (Thermo Fisher Scientific, 31966-021) supplemented with 10% fetal bovine serum (ThermoFisher Scientific, 10270-106) and FACS was performed. Samples were sorted on a FacsAria flow cytometer (BD Biosciences) and gated to exclude debris and cell clumps and sorted for Venus$^+$ cells. Approximately 75,000 Venus$^+$ cells were collected and used as input for ATAC-seq. Nucleus preparation, transposition reaction, and library amplification were performed as previously described (35). In short, cells were washed in phosphate buffered saline and lysed in cold lysis buffer (10 mM Tris·Cl, pH 7.4, 10 mM NaCl, 3 mM $MgCl_2$, 0.1% [vol/vol] Igepal CA-630). Transposition reaction was performed as described using the Nextera DNA Library Prep kit (Illumina, FC-121-1030) for 30 min, followed by cleanup using the MinElute PCR Purification Kit (Qiagen, 28004). Transposed DNA fragments were amplified using NEBNext High-Fidelity 2× PCR Master Mix (New England Biolabs, M0541) with custom barcoded PCR primers (sequences as described in ref. 35). The amplified library was purified using the MinElute PCR Purification Kit (Qiagen, 28004). The library was sequenced (paired-end 125 bp) and data collected on a HiSeq 2500.

ACKNOWLEDGMENTS. We thank Jaco Hagoort for his assistance with the AMIRA 3D reconstructions, Dr. Vasanth Vedantham for advice on the laser capture microdissection protocol, and Joyce Man for help with figures. This work was supported by Fondation Leducq (Grant 14CVD01, to V.M.C.), and by the Dutch Heart Foundation (Grant 2016T047 to B.J.B. and Cardiovasculair Onderzoek Nederland Project 2014-18 CONCOR-genes, to J.B. and V.M.C.).

1. V. W. W. van Eif, H. D. Devalla, G. J. J. Boink, V. M. Christoffels, Transcriptional regulation of the cardiac conduction system. *Nat. Rev. Cardiol.* **15**, 617–630 (2018).
2. A. Pfeufer *et al*., Genome-wide association study of PR interval. *Nat. Genet.* **42**, 153–159 (2010).
3. N. Sotoodehnia *et al*., Common variants in 22 loci are associated with QRS duration and cardiac ventricular conduction. *Nat. Genet.* **42**, 1068–1076 (2010).
4. N. Verweij *et al*., Genetic determinants of P wave duration and PR segment. *Circ. Cardiovasc. Genet.* **7**, 475–481 (2014).
5. P. van der Harst *et al*., 52 genetic loci influencing Myocardial Mass. *J. Am. Coll. Cardiol.* **68**, 1435–1448 (2016).
6. J. van Setten *et al*., PR interval genome-wide association meta-analysis identifies 50 loci associated with atrial and atrioventricular electrical activity. *Nat. Commun.* **9**, 2904 (2018).
7. J. R. Dixon *et al*., Topological domains in mammalian genomes identified by analysis of chromatin interactions. *Nature* **485**, 376–380 (2012).
8. H. K. Long, S. L. Prescott, J. Wysocka, Ever-changing landscapes: Transcriptional enhancers in development and evolution. *Cell* **167**, 1170–1187 (2016).
9. E. P. Nora *et al*., Spatial partitioning of the regulatory landscape of the X-inactivation centre. *Nature* **485**, 381–385 (2012).
10. S. S. Rao *et al*., A 3D map of the human genome at kilobase resolution reveals principles of chromatin looping. *Cell* **159**, 1665–1680 (2014).
11. P. H. Krijger, W. de Laat, Regulation of disease-associated gene expression in the 3D genome. *Nat. Rev. Mol. Cell Biol.* **17**, 771–782 (2016).
12. J. H. van Weerd *et al*., A large permissive regulatory domain exclusively controls Tbx3 expression in the cardiac conduction system. *Circ. Res.* **115**, 432–441 (2014).
13. N. V. Munshi, Gene regulatory networks in cardiac conduction system development. *Circ. Res.* **110**, 1525–1537 (2012).
14. D. S. Park, G. I. Fishman, Development and function of the cardiac conduction system in health and disease. *J. Cardiovasc. Dev. Dis.* **4**, 7 (2017).
15. I. D. Greener *et al*., Molecular architecture of the human specialised atrioventricular conduction axis. *J. Mol. Cell. Cardiol.* **50**, 642–651 (2011).
16. W. T. Aanhaanen *et al*., Developmental origin, growth, and three-dimensional architecture of the atrioventricular conduction axis of the mouse heart. *Circ. Res.* **107**, 728–736 (2010).
17. M. E. Mangoni *et al*., Bradycardia and slowing of the atrioventricular conduction in mice lacking CaV3.1/alpha1G T-type calcium channels. *Circ. Res.* **98**, 1422–1430 (2006).
18. X. Liang *et al*., HCN4 dynamically marks the first heart field and conduction system precursors. *Circ. Res.* **113**, 399–407 (2013).
19. M. Wu, S. Peng, Y. Zhao, Inducible gene deletion in the entire cardiac conduction system using Hcn4-CreERT2 BAC transgenic mice. *Genesis* **52**, 134–140 (2014).
20. L. Miquerol *et al*., Architectural and functional asymmetry of the His-Purkinje system of the murine heart. *Cardiovasc. Res.* **63**, 77–86 (2004).
21. R. A. Mohan *et al*., Embryonic Tbx3$^+$ cardiomyocytes form the mature cardiac conduction system by progressive fate restriction. *Development* **145**, 1–12 (2018).
22. T. Horsthuis *et al*., Gene expression profiling of the forming atrioventricular node using a novel tbx3-based node-specific transgenic reporter. *Circ. Res.* **105**, 61–69 (2009).
23. W. R. Goodyer *et al*., Transcriptomic profiling of the developing cardiac conduction system at single-cell resolution. *Circ. Res.* **125**, 379–397 (2019).
24. C. Marionneau *et al*., Specific pattern of ionic channel gene expression associated with pacemaker activity in the mouse heart. *J. Physiol.* **562**, 223–234 (2005).
25. L. Miquerol *et al*., Resolving cell lineage contributions to the ventricular conduction system with a Cx40-GFP allele: A dual contribution of the first and second heart fields. *Dev. Dyn.* **242**, 665–677 (2013).
26. S. Rentschler *et al*., Notch signaling regulates murine atrioventricular conduction and the formation of accessory pathways. *J. Clin. Invest.* **121**, 525–533 (2011).
27. M. C. Verhoeven, C. Haase, V. M. Christoffels, G. Weidinger, J. Bakkers, Wnt signaling regulates atrioventricular canal formation upstream of BMP and Tbx2. *Birth Defects Res. A Clin. Mol. Teratol.* **91**, 435–440 (2011).
28. B. S. Gillers *et al*., Canonical wnt signaling regulates atrioventricular junction programming and electrophysiological properties. *Circ. Res.* **116**, 398–406 (2015).
29. S. Virágh, C. E. Challice, The development of the conduction system in the mouse embryo heart. *Dev. Biol.* **89**, 25–40 (1982).
30. E. D. Canale, G. R. Campbell, J. J. Smolich, J. H. Campbell, *Cardiac muscle*, (Springer Verlag, Berlin, 1986).
31. R. L. Dehaan, Differentiation of the atrioventricular conducting system of the heart. *Circulation* **24**, 458–470 (1961).
32. S. A. Lambert *et al*., The human transcription factors. *Cell* **172**, 650–665 (2018).
33. I. P. G. Moskowitz *et al*., The T-Box transcription factor Tbx5 is required for the patterning and maturation of the murine cardiac conduction system. *Development* **131**, 4107–4116 (2004).
34. C. A. Risebro *et al*., Prox1 maintains muscle structure and growth in the developing heart. *Development* **136**, 495–505 (2009).
35. J. D. Buenrostro, P. G. Giresi, L. C. Zaba, H. Y. Chang, W. J. Greenleaf, Transposition of native chromatin for fast and sensitive epigenomic profiling of open chromatin, DNA-binding proteins and nucleosome position. *Nat. Methods* **10**, 1213–1218 (2013).
36. S. Preissl *et al*., Deciphering the epigenetic code of cardiac myocyte transcription. *Circ. Res.* **117**, 413–423 (2015).
37. K. van Duijvenboden *et al*., Conserved NPPB+ border zone switches from MEF2- to AP-1-driven gene program. *Circulation* **140**, 864–879 (2019).
38. R. Singh *et al*., Tbx20 interacts with smads to confine tbx2 expression to the atrioventricular canal. *Circ. Res.* **105**, 442–452 (2009).
39. N. V. Munshi *et al*., Cx30.2 enhancer analysis identifies Gata4 as a novel regulator of atrioventricular delay. *Development* **136**, 2665–2674 (2009).
40. A. F. van Ouwerkerk *et al*., Identification of atrial fibrillation associated genes and functional non-coding variants. *Nat. Commun.* **10**, 4755 (2019).
41. M. van den Boogaard *et al*., Genetic variation in T-box binding element functionally affects SCN5A/SCN10A enhancer. *J. Clin. Invest.* **122**, 2519–2530 (2012).
42. L. Luna-Zurita *et al*., Complex interdependence regulates heterotypic transcription factor distribution and coordinates Cardiogenesis. *Cell* **164**, 999–1014 (2016).
43. K. van Duijvenboden, B. A. de Boer, N. Capon, J. M. Ruijter, V. M. Christoffels, EMERGE: A flexible modelling framework to predict genomic regulatory elements from genomic signatures. *Nucleic Acids Res.* **44**, e42 (2016).
44. J. H. Cartwright *et al*, Multi-ancestry GWAS of the electrocardiographic PR interval identifies 210 loci underlying cardiac conduction. bioRxiv:10.1101/712398 (24 July 2019), p 53.
45. A. P. Landstrom, D. Dobrev, X. H. T. Wehrens, Calcium signaling and cardiac arrhythmias. *Circ. Res.* **120**, 1969–1993 (2017).
46. N. J. Chandler *et al*., Molecular architecture of the human sinus node: Insights into the function of the cardiac pacemaker. *Circulation* **119**, 1562–1575 (2009).
47. W. M. Hoogaars *et al*., Tbx3 controls the sinoatrial node gene program and imposes pacemaker function on the atria. *Genes Dev.* **21**, 1098–1112 (2007).
48. S. Stefanovic *et al*., GATA-dependent regulatory switches establish atrioventricular canal specificity during heart development. *Nat. Commun.* **5**, 3680 (2014).
49. I. P. Moskowitz *et al*., A molecular pathway including Id2, Tbx5, and Nkx2-5 required for cardiac conduction system development. *Cell* **129**, 1365–1376 (2007).
50. G. Cheng *et al*., Development of the cardiac conduction system involves recruitment within a multipotent cardiomyogenic lineage. *Development* **126**, 5041–5049 (1999).
51. M. L. Bakker *et al*., Transcription factor Tbx3 is required for the specification of the atrioventricular conduction system. *Circ. Res.* **102**, 1340–1349 (2008).
52. M. H. Soonpaa, K. K. Kim, L. Pajak, M. Franklin, L. J. Field, Cardiomyocyte DNA synthesis and binucleation during murine development. *Am. J. Physiol.* **271**, H2183–H2189 (1996).
53. K. Alkass *et al*., No evidence for cardiomyocyte number expansion in preadolescent mice. *Cell* **163**, 1026–1036 (2015).
54. M. H. Soonpaa *et al*., Cardiomyocyte cell-cycle activity during preadolescence. *Cell* **163**, 781–782 (2015).

55. D. U. Frank *et al*., Lethal arrhythmias in Tbx3-deficient mice reveal extreme dosage sensitivity of cardiac conduction system function and homeostasis. *Proc. Natl. Acad. Sci. U.S.A.* **109**, E154–E163 (2012).
56. W. T. Aanhaanen *et al*., Defective Tbx2-dependent patterning of the atrioventricular canal myocardium causes accessory pathway formation in mice. *J. Clin. Invest.* **121**, 534–544 (2011).
57. H. H. Nguyen, D. K. Grange, M. C. Johnson, G. F. Van Hare, P. Y. Jay, Dichotomous roles of *TBX3* in the establishment of atrioventricular conduction pathways in the human heart. *HeartRhythm Case Rep.* **5**, 109–111 (2018).
58. L. Fabritz *et al*., Autonomic modulation and antiarrhythmic therapy in a model of long QT syndrome type 3. *Cardiovasc. Res.* **87**, 60–72 (2010).
59. W. M. Hoogaars *et al*., The transcriptional repressor Tbx3 delineates the developing central conduction system of the heart. *Cardiovasc. Res.* **62**, 489–499 (2004).
60. A. D. Mori *et al*., Tbx5-dependent rheostatic control of cardiac gene expression and morphogenesis. *Dev. Biol.* **297**, 566–586 (2006).
61. D. E. Arnolds *et al*., TBX5 drives Scn5a expression to regulate cardiac conduction system function. *J. Clin. Invest.* **122**, 2509–2518 (2012).
62. M. Bamshad *et al*., Mutations in human TBX3 alter limb, apocrine and genital development in ulnar-mammary syndrome. *Nat. Genet.* **16**, 311–315 (1997).
63. O. Burnicka-Turek *et al*., Transcriptional patterning of the ventricular cardiac conduction system. *Circ. Res.*, 10.1161/CIRCRESAHA.118.314460 (2020).
64. R. Singh *et al*., Tbx2 and Tbx3 induce atrioventricular myocardial development and endocardial cushion formation. *Cell. Mol. Life Sci.* **69**, 1377–1389 (2012).
65. Ml. He, L. Wen, C. E. Campbell, J. Y. Wu, Y. Rao, Transcription repression by Xenopus ET and its human ortholog TBX3, a gene involved in ulnar-mammary syndrome. *Proc. Natl. Acad. Sci. U.S.A.* **96**, 10212–10217 (1999).
66. M. Osterwalder *et al*., Enhancer redundancy provides phenotypic robustness in mammalian development. *Nature* **554**, 239–243 (2018).